A Fast Phase Space Method for Computing Creeping Rays

Mohammad Motamed, Olof Runborg

Department of Numerical Analysis and Computer Science,
Royal Institute of Technology (KTH),
10044 Stockholm, Sweden
E-mail: mohamad@nada.kth.se, olofr@nada.kth.se

Abstract

Creeping rays can give an important contribution to the solution of medium to high frequency scattering problems. They are generated at the shadow lines of the illuminated scatterer by grazing incident rays and propagate along geodesics on the scatterer surface, continuously shedding diffracted rays in their tangential direction.

In this paper we show how the ray propagation problem can be formulated as a partial differential equation (PDE) in a three-dimensional phase space. To solve the PDE we use a fast marching method. The PDE solution contains information about all possible creeping rays. This information includes the phase and amplitude of the field, which are extracted by a fast postprocessing. Computationally the cost of solving the PDE is less than tracing all rays individually by solving a system of ordinary differential equations.

We consider an application to monostatic radar cross section problems where creeping rays from all illumination angles must be computed. The numerical results of the fast phase space method and a comparison with the results of ray tracing are presented.

1   Introduction

The general problem that we are interested in is the scattering of a time-harmonic incident field by a bounded scatterer D. If the total field is split into an incident and a scattered field, this can be formulated as a boundary value problem for the scattered field in the region outside D, consisting of the Helmholtz equation,

$$\Delta W + n(\mathbf{x})^2 \omega^2 W = 0, \qquad \mathbf{x} \in \mathbb{R}^3 \setminus \bar{D}, \tag{1}$$

augmented with Dirichlet, Neumann or Robin boundary conditions on the boundary of the scatterer ∂D, and the Sommerfeld radiation condition at infinity. Here $n(\mathbf{x})$ is the index of refraction, and ω is the angular frequency.

In direct numerical simulations of (1) the accuracy of the solution is determined by the number of grid points or elements per wave length. The computational cost to maintain constant accuracy grows algebraically with the frequency, and for sufficiently high frequencies, a direct numerical simulation is no longer feasible. Numerical methods based on approximations of (1) are needed.

Fortunately, there exist good such approximations precisely for the difficult case of high frequency solutions. In free space, a typical high frequency solution can be approximated by a simple wave,

$$W(\mathbf{x}) \approx a(\mathbf{x}) e^{i\omega \phi(\mathbf{x})}, \qquad \mathbf{x} \in \mathbb{R}^3 \tag{2}$$

where the amplitude $a(\mathbf{x})$ and the phase function $\phi(\mathbf{x})$ depend only mildly on the parameter ω and vary on a much coarser scale than $W(\mathbf{x})$ itself. Geometrical optics (GO) considers the case when $\omega \to \infty$. The frequency then disappears from the model and the equations can be solved at a computational cost independent of ω. GO can be formulated as the partial differential equations for ϕ and a. The phase function ϕ satisfies the *eikonal equation*,

$$|\nabla \phi| = n(x), \tag{3}$$

and the leading order amplitude term a satisfies the *transport equation*,

$$2\nabla\phi \cdot \nabla a + \Delta\phi a = 0. \tag{4}$$

GO can also be formulated in terms of ordinary differential equations (ODE). It corresponds to solving the eikonal equation (3) through the method of characteristics, i.e. solving the system of ODEs,

$$\frac{d\mathbf{x}}{dt} = \nabla_p H(\mathbf{x}, \mathbf{p}), \qquad \frac{d\mathbf{p}}{dt} = -\nabla_x H(\mathbf{x}, \mathbf{p}), \qquad H(\mathbf{x}, \mathbf{p}) = \frac{|\mathbf{p}|}{n(\mathbf{x})}, \tag{5}$$

where t is time. As long as ϕ is smooth, the relationship between the models is given by $\phi(\mathbf{x}(t)) = \phi(\mathbf{x}(0)) + t$. There are also ODEs giving the amplitude $a(\mathbf{x}(t))$ along the characteristics.

The main drawbacks of the infinite frequency approximation of geometrical optics are that diffraction effects at boundaries are lost, and that the approximation breaks down at caustics, where the predicted amplitude a is unbounded. Geometrical theory of diffraction (GTD), pioneered by J. Keller in 1960s, adds diffraction effects to the GO approximations. One type of diffracted rays are *creeping rays*, which are generated at the *shadow line* of the scatterer, i.e. where the incident ray strikes the surface of the scatterer at grazing angle. At this point the incident ray divides into two parts: one part continues straight on, and a second part propagates along geodesics on the surface, continuously shedding diffracted rays in its tangential direction. See Figure 1. In analogy with (2), a wave field is generated on the surface

$$W_s(\mathbf{u}) = a(\mathbf{u})e^{i\omega\phi(\mathbf{u})}, \tag{6}$$

where $\phi(\mathbf{u})$ and $a(\mathbf{u})$ are now the surface phase and amplitude and $\mathbf{u} \in \mathbb{R}^2$ is a parameterization of the surface. The creeping rays satisfy a system of ODEs similar to (5). They are related to (6) in the same way as the standard GO rays are related to (2).

Creeping rays can give an important contribution to the solution at medium to high frequencies, for instance in radar cross section (RCS) computations for low observable objects [3] and in antenna coupling problems [15]. We want to compute the creeping rays and the associated wave field in (6).

Various methods have been devised to compute the geometrical optics solution. They can be divided into Lagrangian and Eulerian methods.
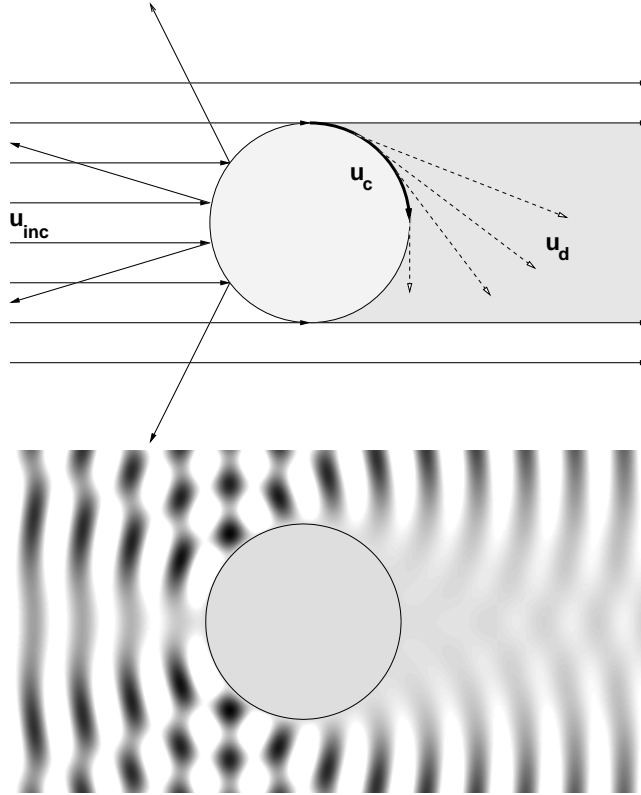
Figure 1: Diffraction by a smooth cylinder. Top figure shows the solution schematically. The incident field u_{inc} induces a creeping ray u_{c} at the north (and south) pole of the cylinder, where the incident direction is orthogonal to the surface normal. As the creeping ray propagates along the surface, it continuously emits surface-diffracted rays u_{d} with exponentially decreasing initial amplitude. Bottom figure shows real part of a solution to the Helmholtz equation. The surface diffracted waves can be seen behind the cylinder.

Lagrangian methods are based on the ODE formulation (5). The simplest Lagragian method is standard ray tracing where the ODEs in (5) togheter with ODEs for the amplitude are solved directly with numerical methods for ODEs. This approach is very common in standard free space GO, [4, 18], but is also done for the creeping ray case, [12, 21]. Ray tracing gives the phase and amplitude solution along a ray, and interpolation must be applied to obtain those quantities everywhere. This can be rather difficult, in particular in regions where rays cross. Another problem with ray tracing is that it may produce diverging rays that fail to cover the domain. Even for smooth $n(\mathbf{x})$ there may be shadow zones where the field is hard to resolve. The interpolation can be simplified by instead

using so-called wave front methods [28, 11]. They are related to ray tracing, but instead of individual rays, an interface representing a wave front is evolved according to the ray equations.

More recently, Eulerian methods based on PDEs have been proposed to avoid some of the drawbacks of ray tracing. These methods discretize the PDEs on fixed computational grids to control accuracy everywhere and there is no need for interpolation. The simplest Eulerian methods solves the eikonal and transport equations (3,4). This technique has been used in standard GO, [27, 26, 7] and also in the surface case, [14]. However, the eikonal and transport equations only give the correct solution when it is a single wave of the form (2). When there are crossing waves, more elaborate schemes must be devised. In the free space GO case a number of methods have been developed in the last ten years using different approaches. Many of them are based on a third formulation of geometrical optics as a kinetic equation set in phase space. They include "big" raytracing [1], patching together multiple eikonal solutions [2], moment methods [22, 23, 9], segment projection method [6], level set methods [20], slowness matching [24], the phase flow method [16] and fast phase space methods [8]. A survey of this research effort is given in [5].

These more advanced methods have so far not been used for the creeping ray case. In this paper we propose an adaptation of the fast phase space method of Fomel and Sethian [8] to this case. This method is computionally expensive if only a few solutions are computed. It becomes attractive when the solution is sought for many different sources but with the same index of refraction. In the creeping ray case this happens for instance when the solution for all illumination angles of a fixed scatterer is of interest. We consider one such example: computing the monostatic RCS.

Following [8] we formulate the ray propagation problem as a time-independent partial differential equation (PDE) in a three-dimensional phase space. We use a fast marching method to solve the PDE. The PDE solution contains information for all incidence angles. The phase and amplitude of the field are extracted by a fast post-processing. Computationally the cost of solving the PDE is less than tracing all rays individually. If the surface is discretized by N^2 points the complexity is $\mathcal{O}(N^3 \log N)$, while ray tracing would cost $\mathcal{O}(N^4)$ if a comparable number of incidence angles (N^2) and rays per angle (N) are considered.

In Section 2, we formulate the governing equations. The numerical method for solving the equations are discussed in Section 3. In Section 4 we show how to extract the information for a particular ray through post-processing. An application to a monostatic RCS problem is shown as an example in Section 5.

2   Governing Equations

For simplicity we consider the case when the scatterer surface has an explicit parameterization. Let $\bar{X}$ be a regular hypersurface, representing a scatterer surface, with the parametric equations $\bar{X} = \bar{X}(\mathbf{u})$, where $\bar{X} = (x, y, z) \in \mathbb{R}^3$ is the coordinate in 3D physical space, and the parameters $\mathbf{u} = (u, v)$ belong to

4

a bounded set $\Omega \subset \mathbb{R}^2$. Let the scatterer be illuminated by incident rays in a direction represented by a normalized vector $\hat{I} = [\iota_1, \iota_2, \iota_3]$. The shadow line is then defined as the set of points where

$$\hat{N}^\top \hat{I} = 0, \tag{7}$$

where $\hat{N}(\mathbf{u})$ is the surface normal at $\bar{X}(\mathbf{u})$,

$$\hat{N} = \frac{\bar{X}_u \times \bar{X}_v}{|\bar{X}_u \times \bar{X}_v|}. \tag{8}$$

Here the subscripts denote differentiation with respect to u and v. We will assume that (7) defines a curve in parameter space, which we denote $\mathbf{u}_0(s)$, and s is the arc length parameterization.

2.1 Geodesics

We start by deriving the equations for creeping rays, which are indeed geodesics on the scatterer surface. According to Keller and Lewis [13], the surface phase satisfies the *surface eikonal equation*,

$$|\tilde{\nabla}\phi| = n, \tag{9}$$

where $n(\mathbf{u})$ is the index of refraction at the surface, and $\tilde{\nabla}$ is the surface gradient, defined as

$$\tilde{\nabla}\phi := JG^{-1}\nabla\phi, \qquad G = J^\top J,$$

with

$$J = [\bar{X}_u \ \bar{X}_v] \in \mathbb{R}^{3\times 2}.$$

We prescribe boundary conditions for (9) on the shadow line, which acts as the source for the creeping rays. The boundary condition is that the surface phase agrees with ϕ_{inc}, the phase of the incoming wave,

$$\phi(\mathbf{u}_0(s)) = \phi_0(\mathbf{u}_0) := \phi_{\text{inc}}(\bar{X}(\mathbf{u}_0(s))), \tag{10}$$

To avoid ambiguities as to which direction the surface waves propagate, we add the condition

$$\tilde{\nabla}\phi(\mathbf{u}_0(s)) = \nabla\phi_{\text{inc}}(\bar{X}(\mathbf{u}_0(s))), \tag{11}$$

which is consistent with (9) since ϕ_{inc} satisfies the free space eikonal equation (3) and with (10) since

$$\frac{d}{ds}\left(\phi(\mathbf{u}_0(s)) - \phi_{\text{inc}}(\bar{X}(\mathbf{u}_0(s)))\right) = \nabla\phi^\top \mathbf{u}_0' - \nabla\phi_{\text{inc}}^\top \frac{d\bar{X}}{ds}$$
$$= (J^\top \tilde{\nabla}\phi)^\top \mathbf{u}_0' - \nabla\phi_{\text{inc}}^\top \frac{d\bar{X}}{ds} = (\tilde{\nabla}\phi - \nabla\phi_{\text{inc}})^\top \frac{d\bar{X}}{ds}.$$

5

In the case when $n = 1$ and the incoming wave is a plane wave in direction $\hat{I}$, we have $\phi_{\text{inc}}(\mathbf{x}) = \hat{I}^\top \mathbf{x}$. Then (10,11) reduce to

$$\phi_0(\mathbf{u}_0(s)) := \hat{I}^\top \bar{X}(\mathbf{u}_0(s)), \qquad \tilde{\nabla}\phi(\mathbf{u}_0(s)) = \hat{I}. \tag{12}$$

We can write (9) as a Hamilton-Jacobi equation $H(\mathbf{u}, \nabla\phi) = 0$, with the Hamiltonian

$$H(\mathbf{u}, \mathbf{p}) \equiv \frac{1}{2}\,\mathbf{p}^\top\, G^{-1}(\mathbf{u})\,\mathbf{p} - \frac{n^2(\mathbf{u})}{2}.$$

Note that in the case $n = $ constant, the geometrical rays associated with the eikonal equation (3) becomes straight lines. Analogously, for the surface eikonal equation (9), the creeping rays for constant n are geodesics, or shortest paths between two points on the surface. Henceforth, we will assume $n \equiv 1$ and a plane incoming wave.

Introducing a parameter τ, the bicharacteristics $\big(\mathbf{u}(\tau), \mathbf{p}(\tau)\big)$ are determined by the solution of the following Hamiltonian equations

$$\dot{\mathbf{u}} = H_\mathbf{p} = G^{-1}\mathbf{p}, \tag{13a}$$

$$\dot{\mathbf{p}} = -H_\mathbf{u}. \tag{13b}$$

Here the dot denotes differentiation with respect to the parameter τ. At the shadow line, the initial direction of the geodesic should be parallel to the incident field. We demand that

$$\frac{d}{d\tau}\bar{X}(\mathbf{u}(\tau))\Big|_{\tau=0} = \hat{I}.$$

This implies that $\mathbf{p}(0) = G\dot{\mathbf{u}}(0) = J^\top J\dot{\mathbf{u}}(0) = J^\top \dot{\bar{X}}(0) = J^\top \hat{I}$. The initial condition for the system (13) therefore reads,

$$\mathbf{u}(0) = \mathbf{u}_0(s), \tag{14a}$$

$$\mathbf{p}(0) = \mathbf{p}_0(s) := J^\top(\mathbf{u}_0(s))\,\hat{I}. \tag{14b}$$

We note that by (12),

$$\mathbf{p}(0) = J^\top(\mathbf{u}_0(s))\,\tilde{\nabla}\phi(\mathbf{u}_0(s)) = J^\top J G^{-1}\nabla\phi(\mathbf{u}_0(s)) = \nabla\phi(\mathbf{u}(0)).$$

As for any Hamiltonian system it therefore follows that

$$\mathbf{p}(\tau) = \nabla\phi(\mathbf{u}(\tau)), \tag{15}$$

for all $\tau \geq 0$, as long as ϕ is smooth. As a consequence, (13) and (15) give

$$|\dot{\bar{X}}| = \left|\frac{d\bar{X}}{d\tau}\right| = |J\dot{\mathbf{u}}| = |J H_\mathbf{p}| = |J G^{-1}\mathbf{p}| = 1, \tag{16}$$

and we can identify the parameter τ with arc length along the creeping rays $\bar{X}(\mathbf{u}(\tau))$. In this case, the system of four first-order ODEs (13) can be written as a system of two second-order equations [13],

$$\ddot{u} + \Gamma_{11}^1 \dot{u}^2 + 2\Gamma_{12}^1 \dot{u}\dot{v} + \Gamma_{22}^1 \dot{v}^2 = 0, \tag{17a}$$

$$\ddot{v} + \Gamma_{11}^2 \dot{u}^2 + 2\Gamma_{12}^2 \dot{u}\dot{v} + \Gamma_{22}^2 \dot{v}^2 = 0. \tag{17b}$$

6

Here $\Gamma_{ij}^k(\mathbf{u})$ are Christoffel symbols, defined by

$$\Gamma_{ij}^k = \sum_{m=1}^{2} \frac{1}{2} g^{km}[(g_{jm})_i + (g_{im})_j - (g_{ji})_m],$$

where $(g_{ij}) = G$ and $(g^{ij}) = G^{-1}$, and subscripts 1 and 2 denote differentiation with respect to u and v, respectively.

Now if we set $\dot{u} = \frac{du}{d\tau} = \rho \cos\theta$ and $\dot{v} = \frac{dv}{d\tau} = \rho \sin\theta$, then $\dot{v} = \dot{u}\tan\theta$, and by differentiating with respect to τ,

$$\ddot{v} = \ddot{u}\tan\theta + \dot{u}\frac{1}{\cos^2\theta}\dot{\theta}. \tag{18}$$

Moreover by (16),

$$\rho = \rho(u,v,\theta) = \left| J \left(\begin{array}{c} \cos\theta \\ \sin\theta \end{array} \right) \right|^{-1} = \left| \bar{X}_u \cos\theta + \bar{X}_v \sin\theta \right|^{-1}.$$

Let $\gamma := (u,v,\theta)$. Using (18), we get

$$\dot{\theta} = \rho(\gamma)\,\mathcal{V}(\gamma),$$

where

$$\mathcal{V}(\gamma) := \rho\Big((\Gamma_{11}^1 \cos^2\theta + 2\Gamma_{12}^1 \cos\theta\sin\theta + \Gamma_{22}^1 \sin^2\theta)\sin\theta -$$

$$(\Gamma_{11}^2 \cos^2\theta + 2\Gamma_{12}^2 \cos\theta\sin\theta + \Gamma_{22}^2 \sin^2\theta)\cos\theta\Big).$$

Therefore the system of ODEs (17), for geodesics, reduces to

$$\left(\begin{array}{c} \dot{u} \\ \dot{v} \\ \dot{\theta} \end{array} \right) = \left(\begin{array}{c} \rho(\gamma)\,\cos\theta \\ \rho(\gamma)\,\sin\theta \\ \rho(\gamma)\,\mathcal{V}(\gamma) \end{array} \right) =: \mathbf{g}(\gamma). \tag{19}$$

2.2 Phase and Amplitude

Let us now derive the ODEs for the surface phase ϕ and amplitude a. As before, we parametrize the creeping ray with the arc length τ in the physical space. In the surface field acossiated with the creeping ray (6), the phase function $\phi(\mathbf{u}(\tau))$ and the amplitude $a(\mathbf{u}(\tau))$ of the field vary with the distance τ along the ray.

From (13) and (15) it follows that the phase of the geodesic satisfies the ODE,

$$\frac{d\phi(\mathbf{u}(\tau))}{d\tau} = \nabla\phi \cdot \dot{\mathbf{u}} = \nabla\phi \cdot G^{-1}\nabla\phi = |\tilde{\nabla}\phi|^2 = 1, \qquad \phi(0) = \phi_0(\mathbf{u}_0). \tag{20}$$

Hence, the phase is the length of the ray.

Now consider a narrow strip of a creeping ray, starting at the incident point Q_0 on the shadow line and propagating along a geodesic on the scatterer surface. See Figure 2.
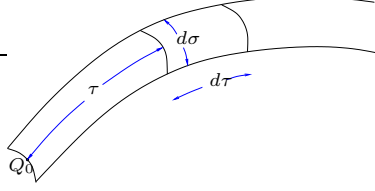
Figure 2: A narrow strip of a creeping ray on the surface.

To determine an equation for the amplitude, we apply the optical form of energy conservation principle in a small interval from τ to $\tau + d\tau$, [17], and get

$$\frac{d}{d\tau}[a(\tau)^2 \, d\sigma(\tau)] = -2\,\alpha(\tau)\,[a(\tau)^2 \, d\sigma(\tau)], \tag{21}$$

where $d\sigma(\tau)$ is the width of the strip at distance τ from Q_0, and $\alpha(\tau)$ is an attenuation factor. Solving (21) gives us

$$a(\tau) = a_0 (\frac{d\sigma_0}{d\sigma})^{\frac{1}{2}} \exp\left(-\int_0^\tau \alpha(r)dr\right), \tag{22}$$

where a_0 and $d\sigma_0$ are the amplitude and strip width at Q_0, respectively. There are thus two parts in this equation which we can treat separately: the attenuation, represented by the exponential, and the geometrical spreading of the creeping ray, represented by $\frac{d\sigma}{d\sigma_0}$.

2.2.1 Attenuation

We will here show that the attenuation can be obtained by solving an ODE coupled to the geodesic system (19).

The attenuation factor α is given by, [17, 19],

$$\alpha = \frac{q_0}{\rho_g} \exp\left(i\frac{\pi}{6}\left(\frac{\omega\rho_g}{2}\right)^{1/3}\right) := \omega^{1/3}\tilde{\alpha}.$$

Here $q_0 \approx 2.33811$ is the smallest positive zero of the Airy function, and ρ_g is the radius of curvature of the surface with respect to arc length along the ray trajectory, given by [10],

$$\rho_g = \frac{1}{-\hat{T}^\top D_{\mathbf{u}}\hat{N}\,\dot{\mathbf{u}}}, \qquad \hat{T} = \frac{d\bar{X}}{d\tau}(\mathbf{u}(\tau)) = J\dot{\mathbf{u}}.$$

Here, $\hat{T}$ is the tangent vector to the surface in the geodesic's direction, and $D_{\mathbf{u}}\hat{N} = [\hat{N}_u\ \hat{N}_v]$ is the Jacobian of the normal vector $\hat{N}$. Note that $|\hat{T}| = 1$ by (16). Since $\hat{T}$, $\hat{N}$ and $\dot{\mathbf{u}}$ are functions of (u, v, θ), so is $\tilde{\alpha} = \tilde{\alpha}(u, v, \theta)$. We can therefore add the ODE

$$\frac{d\beta}{d\tau} = \tilde{\alpha}(u, v, \theta), \qquad \beta(0) = 0, \tag{23}$$
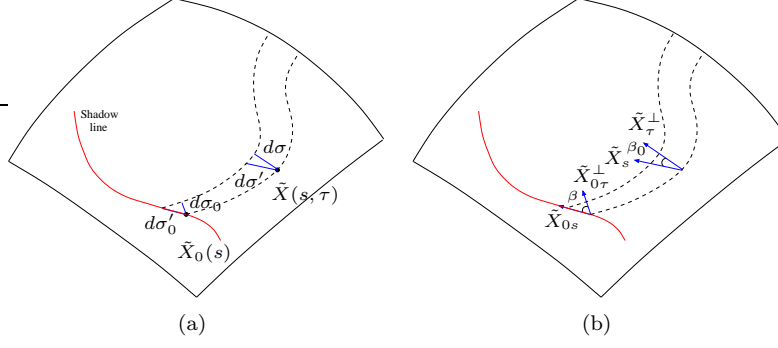
8

Figure 3: Geometrical spreading of a creeping ray on the surface, starting at the shadow line and ending at the boundary.

to the geodesic system (19), and then express the attenuation as

$$\exp\left(-\int_0^\tau \alpha(r)dr\right) = \exp\left(-\omega^{1/3}\beta(\tau)\right).$$

Note that β is independent of the frequency ω.

2.2.2 Geometrical Spreading

To compute the amplitude of the creeping ray from (22), we also need to compute the geometrical spreading. We consider again a narrow strip of a geodesics, as in Figure 2, and let $d\sigma_0(s)$ and $d\sigma(s,\tau)$ be the strip width at the shadow line and at the distance τ from the shadow line, respectively.

Set $\tilde{\mathbf{u}}(s,\tau) := \mathbf{u}(\tau)$, where $(\mathbf{u}(\tau), \mathbf{p}(\tau))$ is a solution to (13) with the initial data (14) so that $\tilde{\mathbf{u}}(s,0) = \mathbf{u}_0(s)$. Moreover, let

$$\tilde{X}(s,\tau) := \bar{X}\big(\tilde{\mathbf{u}}(s,\tau)\big).$$

Then $\tilde{X}$ is the point on the geodesic at the distance τ from the shadow line, and $\tilde{X}_0(s) = \tilde{X}(s,0)$ is the starting point on the shadow line. Denote the geometrical spreading of the creeping ray at the point $\tilde{X}(s,\tau)$ in the physical space by

$$\mathcal{Q}(s,\tau) := \frac{d\sigma(s,\tau)}{d\sigma_0(s)}.$$

Moreover, let $d\sigma_0'$ and $d\sigma'$ be the strip width in the direction of the shadow line, defined by $d\sigma_0' = |\tilde{X}_{0s}|\,ds$ and $d\sigma' = |\tilde{X}_s|\,ds$. See Figure 3.

Then we have

$$\cos\beta_0 = \frac{d\sigma_0}{d\sigma_0'} = \frac{\tilde{X}_{0\tau}^\perp}{|\tilde{X}_{0\tau}^\perp|} \cdot \frac{\tilde{X}_{0s}}{|\tilde{X}_{0s}|}, \tag{24}$$

$$\cos\beta = \frac{d\sigma}{d\sigma'} = \frac{\tilde{X}_\tau^\perp}{|\tilde{X}_\tau^\perp|} \cdot \frac{\tilde{X}_s}{|\tilde{X}_s|}, \tag{25}$$
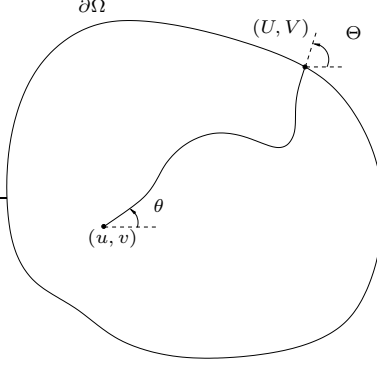
9

Figure 4: A geodesic in the parameter space. The function F is defined as $F(u, v, \theta) = (U, V, \Theta)$, with the notation as in the figure.

where the τ- and s-subscripts denote differentiation along the ray and the shadow line, respectively, and $\tilde{X}_\tau^\perp$ is orthogonal to $\tilde{X}_\tau$ in the tangent plane to the surface. Since $|\tilde{X}_{0\tau}^\perp| = |\tilde{X}_\tau^\perp| = 1$ by (16), the geometrical spreading is then computed as,

$$\mathcal{Q}(s, \tau) = \frac{\tilde{X}_\tau^\perp \cdot \tilde{X}_s}{\tilde{X}_{0\tau}^\perp \cdot \tilde{X}_{0s}}. \tag{26}$$

We will show how to calculate the right hand side of (26) numerically, below.

2.3 Eulerian Formulation

There are a number of drawbacks with Lagrangian methods based on solving the ODEs (19), (20) and (23). In particular, in the regions where rays diverge or cross, interpolation can be difficult. Instead, we use an Eulerian formulation and derive time-independent PDEs, which can be solved on a fixed computational grid.

We introduce the phase space $\mathbb{P} = \mathbb{R}^2 \times \mathbb{S}$, where $\mathbb{S}$ is the periodic sphere. We consider the triplet $\gamma = (u, v, \theta)$ as a point in this space. The geodesics on the scatterer are then confined to a subdomain $\Omega_p = \Omega \times \mathbb{S} \subset \mathbb{P}$ in phase space.

Let us now introduce an unknown function $F : \mathbb{P} \to \mathbb{P}$,

$$F(\gamma) = \begin{pmatrix} U(\gamma) \\ V(\gamma) \\ \Theta(\gamma) \end{pmatrix}, \tag{27}$$

which is the point where the geodesic starting at $\mathbf{u} = (u, v) \in \Omega$ with direction $\theta \in \mathbb{S}$ will cross the boundary of Ω_p. See Figure 4. Since F is constant along a geodesic, we have

$$0 = \frac{d}{d\tau} F(u(\tau), v(\tau), \theta(\tau)) = \frac{du}{d\tau} F_u + \frac{dv}{d\tau} F_v + \frac{d\theta}{d\tau} F_\theta. \tag{28}$$

10

Using (28) and (19), we can write the *escape* PDE for F as

$$\cos\theta\, F_u + \sin\theta\, F_v + \mathcal{V}(\gamma)\, F_\theta = 0, \quad \gamma \in \Omega_p, \tag{29}$$

with the boundary condition at inflow points, i.e., the points on $\partial\Omega_p$ at which geodesics are out-going,

$$F(\gamma) = \gamma, \qquad \gamma \in \partial\Omega_p^{\text{inflow}}.$$

Note that inflowing characteristics correspond to out-going geodesics.

Now we define a surface phase $\Phi : \mathbb{P} \to \mathbb{R}$, such that $\Phi(\gamma)$ is the distance traveled by a geodesic starting at the point $\mathbf{u}$ with direction θ before it hits the boundary of Ω_p. Using (20), we can derive the PDE for Φ as

$$\cos\theta\, \Phi_u + \sin\theta\, \Phi_v + \mathcal{V}(\gamma)\, \Phi_\theta = \frac{1}{\rho(\gamma)}, \quad \gamma \in \Omega_p, \tag{30}$$

with the boundary condition at inflow points

$$\Phi(\gamma) = 0, \qquad \gamma \in \partial\Omega_p^{\text{inflow}}.$$

In the same way we define a function $B : \mathbb{P} \to \mathbb{R}$ as the β-value of a geodesic starting at the point $\gamma \in \Omega_p$ when it hits the boundary of Ω_p. We then use (23) and derive the PDE for B as

$$\cos\theta\, B_u + \sin\theta\, B_v + \mathcal{V}(\gamma)\, B_\theta = \frac{\tilde{\alpha}(\gamma)}{\rho(\gamma)}, \quad \gamma \in \Omega_p, \tag{31}$$

with the boundary condition at inflow points

$$B(\gamma) = 0, \qquad \gamma \in \partial\Omega_p^{\text{inflow}}.$$

For the geometrical spreading we consider a fixed shadowline $\gamma_0(s) = (u_0(s), v_0(s), \theta_0(s))$ and like in Section 2.2.2 we define

$$\tilde{u}(s,\tau) = u(\tau), \qquad \tilde{v}(s,\tau) = v(\tau), \qquad \tilde{\theta}(s,\tau) = \theta(\tau),$$

where (u,v,θ) solves (19) with initial data $(u_0(s), v_0(s), \theta_0(s))$. Setting $\tilde{\gamma} = (\tilde{u}, \tilde{v}, \tilde{\theta})$ we thus have

$$\tilde{\gamma}_\tau = \mathbf{g}(\tilde{\gamma}), \qquad \tilde{\gamma}(s,0) = \gamma_0(s),$$

with $\mathbf{g}$ defined in (19).

For a given shadowline, the creeping rays will lie on a submanifold of phase space $\mathbb{P}$ which we define as $\mathbb{L}(\gamma_0) = \{\tilde{\gamma}(s,\tau) : \tau \geq 0\}$. We then introduce the function $Q : \mathbb{L}(\gamma_0) \to \mathbb{R}$ as

$$Q(\tilde{\gamma}(s,\tau)) := \mathcal{Q}(s,\tau).$$

which is a Eulerian version of the geometrical spreading, restricted to $\mathbb{L}(\gamma_0)$. We will use the following simple Lemma.

11

Lemma 1. *The Jacobian $D_\gamma F(\gamma) \in \mathbb{R}^{3\times3}$ has rank two for all $\gamma \in \Omega_p$ where it is well-defined. Its null space is spanned by $\mathbf{g}(\gamma)$.*

Proof. That $D_\gamma F(\gamma)\mathbf{g}(\gamma) = 0$ is just a restatement of (29). Suppose $D_\gamma F(\gamma)\mathbf{v} = 0$ and construct a curve $\gamma_0(s) \subset \mathbb{P}$ satisfying $\gamma_0(0) = \gamma$ and $\gamma_0'(0) = \mathbf{v}$. Let $\tilde{\gamma}(s, \tau)$ be defined for this curve in the same way as above. Then $\frac{d}{ds}F(\gamma_0(s)) = 0$ for $s = 0$. Moreover, since $D_\gamma F(\gamma)$ is well-defined there is a differentiable function $\hat{\tau}(s)$ such that $F(\gamma_0(s)) = \tilde{\gamma}(s, \hat{\tau}(s))$ in a neighborhood of $s = 0$. Together this means that

$$0 = \frac{d}{ds}\tilde{\gamma}(s, \hat{\tau}(s))\Big|_{s=0} = \tilde{\gamma}_s(0, \hat{\tau}(0)) + \hat{\tau}'(0)\tilde{\gamma}_\tau(0, \hat{\tau}(0)). \tag{32}$$

Since $-\hat{\tau}'(0)\tilde{\gamma}_\tau(0, \tau)$ is a solution to the ODE $(\tilde{\gamma}_s)_\tau = D_\gamma \mathbf{g}(\tilde{\gamma})\tilde{\gamma}_s$ for $s = 0$, uniqueness of ODE solutions implies that (32) holds for all $\tau \geq 0$, in particular

$$\tilde{\gamma}_s(0, 0) + \hat{\tau}'(0)\tilde{\gamma}_\tau(0, 0) = 0 \quad \Leftrightarrow \quad \mathbf{v} = -\hat{\tau}'(0)\mathbf{g}(\gamma).$$

Hence, if $\mathbf{v}$ is in the nullspace, then it is parallel to $\mathbf{g}(\gamma)$, and the nullspace is thus one-dimensional. $\qquad\square$

In order to compute Q we first find a solution $z = z(s, \tau)$ to

$$D_\gamma F(\tilde{\gamma})z = \frac{d}{ds}F(\gamma_0(s)). \tag{33}$$

We note that $F(\tilde{\gamma}(s, \tau)) = F(\gamma_0(s))$ for all $\tau \geq 0$, so this z satisfies

$$D_\gamma F(\tilde{\gamma})z = D_\gamma F(\tilde{\gamma})\tilde{\gamma}_s.$$

By Lemma 1 we therefore get

$$z(s, \tau) = \tilde{\gamma}_s + \alpha\mathbf{g}(\tilde{\gamma}) = \tilde{\gamma}_s + \alpha\tilde{\gamma}_\tau,$$

for some α and since $\tilde{X}_\tau = \hat{T}(\tilde{\gamma})$ by (16), we have

$$[\hat{T}(\tilde{\gamma}) \times \hat{N}(\tilde{u}, \tilde{v})]^\top J(\tilde{u}, \tilde{v})z = \tilde{X}_\tau^\perp \cdot (\tilde{X}_s + \alpha\tilde{X}_\tau) = \tilde{X}_\tau^\perp \cdot \tilde{X}_s.$$

Consequently, since $\hat{T}(\gamma_0(s)) = \hat{I}$,

$$Q(\tilde{\gamma}) = \frac{[\hat{T}(\tilde{\gamma}) \times \hat{N}(\tilde{u}, \tilde{v})]^\top J(\tilde{u}, \tilde{v})z}{[\hat{I} \times \hat{N}(\mathbf{u_0}(s))]^\top \tilde{X}_{0s}(s)}. \tag{34}$$

On the boundary, when $\tilde{\gamma} \in \partial\Omega_p$ we can simplify the computation and avoid solving for z in (33). Let $\hat{X} : \mathbb{R} \to \mathbb{R}^3$ be defined by $\hat{X}(s) := \bar{X}(U(\gamma_0(s)), V(\gamma_0(s)))$ with U, V defined in (27). As in the proof of Lemma 1 there is a function $\hat{\tau}(s)$ such that

$$\hat{X}(s) = \tilde{X}(s, \hat{\tau}(s)). \tag{35}$$

After differentiating (35) with respect to s, we get

$$\hat{X}_s(s) = \tilde{X}_\tau \hat{\tau}'(s) + \tilde{X}_s.$$

12

Therefore, for $\tilde{\gamma}$ on the boundary, i.e. $\tilde{\gamma} = F(\gamma_0)$,

$$Q(\tilde{\gamma}) = \frac{[\hat{T}(\tilde{\gamma}) \times \hat{N}(\tilde{u}, \tilde{v})]^\top \hat{X}_s(s)}{[\hat{I} \times \hat{N}(\mathbf{u_0}(s))]^\top \tilde{X}_{0s}}. \tag{36}$$

Note that $\hat{X}_s(s)$ can easily be computed from the numerical solution to the PDE (29).

3   Numerical Solution of the PDEs

All PDEs (29), (30), and (31) are of the general form

$$af_u + bf_v + cf_\theta = d(u, v, \theta), \tag{37}$$

which are time-independent hyperbolic equations.

In the phase space $\mathbb{P}$, the direction of characteristics at the points on the boundary determines if boundary conditions are needed at that point. We assign boundary conditions at the points where a characteristic is in-going. For example a characteristic is in-going if $\dot{u} = \rho \cos\theta > 0$ on the left boundary and if $\dot{v} = \rho \sin\theta > 0$ on the lower boundary. More precisely, suppose Ω is the unit square and $-\pi < \theta \leq \pi$. Then we prescribe boundary condition on $\partial\Omega_p^{\text{inflow}}$ given by

$$\partial\Omega_p^{\text{inflow}} = \left\{ u = 0, \ |\theta| < \frac{\pi}{2} \right\} \bigcup \left\{ u = 1, \ |\theta - \pi| < \frac{\pi}{2} \right\}$$
$$\bigcup \{ v = 0, \ \theta > 0 \} \bigcup \{ v = 1, \ \theta < 0 \}.$$

We always use periodic boundary conditions in the θ direction.

To solve these equations, we use a Fast Marching algorithm, given by Fomel and Sethian [8]. We let $f = (F, \Phi, B)$ and discretize the phase space domain $\Omega_p = \Omega \times \mathbb{S}$ uniformly, setting $u_i = i\Delta u$, $v_j = j\Delta v$ and $\theta_k = k\Delta\theta$, with the step sizes $\Delta u = \Delta v = \frac{1}{N}$ and $\Delta\theta = \frac{2\pi}{N}$. Then by solving the PDEs (37), we get the approximate solution

$$f_{ijk} = (F_{ijk}, \Phi_{ijk}, B_{ijk}) \approx (F(u_i, v_j, \theta_k), \Phi(u_i, v_j, \theta_k), B(u_i, v_j, \theta_k)).$$

The complexity is $\mathcal{O}(N^3 \log N)$. See [8] for more details.

4   Post-Processing

To extract properties like phase and amplitude for a ray family, post-processing of the solution to the escape PDEs (37) is needed. It is based on the following simple observation. By the uniqueness of solutions of ODEs,

$$F(\gamma_1) = F(\gamma_2),$$

if and only if the points γ_1 and γ_2 lie on the same geodesic.

13

As an example, suppose we want to compute the surface phase at a point on the scatterer, when the scatterer is illuminated. We assume that the shadow line $\gamma_0(s) = (u_0(s), v_0(s), \theta_0(s))$ is known. For each point $(u, v) \in \Omega$ covered by the surface wave there is at least one creeping ray passing that point starting at the shadowline $\gamma_0(s)$. By the argument above, we can thus find $s = s^*(u, v)$ and phase angle $\theta = \theta^*(u, v)$, as the solution to

$$F(\gamma_0(s)) = F(u, v, \theta). \tag{38}$$

The phase at (u, v) is then given by

$$\phi(u, v) = \phi_0(\mathbf{u}_0(s^*)) + \Phi(\gamma_0(s^*)) - \Phi(\gamma^*), \quad \gamma^* = (u, v, \theta^*),$$

with ϕ_0 as in (12). Note that γ^* is now in the submanifold $\mathbb{L}(\gamma_0)$ which was defined in Section 2.3. There may be multiple solutions (s^*, θ^*) to (38), giving multiple phases.

We now introduce a function $A : \mathbb{L}(\gamma_0) \to \mathbb{R}$ as the amplitude at the point $\gamma \in \mathbb{L}(\gamma_0)$ on the geodesic starting at the shadowline $\gamma_0(s)$. By (22) we can write

$$A(\gamma^*) = A_0 \, Q(\gamma^*)^{\frac{-1}{2}} \exp\left(-\omega^{\frac{1}{3}} \left(B(\gamma_0(s^*)) - B(\gamma^*)\right)\right),$$

where A_0 is the amplitude at the point $\gamma_0(s^*)$, and $Q(\gamma^*)$ is computed by (34).

The main difficulty here is to solve (38). We now show how to solve it. Since $F = (U, V, \Theta)$ is a point on the phase space boundary $\partial\Omega_p$, it can be reduced to a point (S, Θ) in $\mathbb{R}^2$. For example in a rectangular domain Ω, Figure 5, we choose $S \in [0, 2\pi]$ along $\partial\Omega$ to be zero at the lower left corner, π at the upper right corner, and 2π again at the lower left corner. Now the left and right hand sides of (38) are curves in $\mathbb{R}^2$ parameterized by s and θ, and solving the algebraic equation (38) amounts to finding crossing points of these curves. See Figure 5.

Numerically, we discretize the parameterization of the shadow line in N grid points $\{s_m\}$, $m = 1, \ldots, N$. For each point $\{\mathbf{u}_0(s_m)\}$ on the parameter space shadow line, the ray direction $\theta_0(s_m)$ at the shadow line is computed using the fact that the tangential vector $\hat{T}$ to the hypersurface at the point $\gamma_0(s_m)$ should be in the same direction as the incident angle $\hat{I}$:

$$\hat{T}(\gamma_0(s_m)) = \hat{I}. \tag{39}$$

After obtaining the discretized phase space shadow line $\{\gamma_0(s_m)\}$, we then interpolate the approximate solution f_{ijk} (available on a regular grid) to find the approximate solution on the shadow line:

$$\tilde{f}_{s_m} = (\tilde{F}_{s_m}, \tilde{\Phi}_{s_m}, \tilde{B}_{s_m}) \approx (F(\gamma_0(s_m)), \Phi(\gamma_0(s_m)), B(\gamma_0(s_m))).$$

Having the discretized solution on the shadowline and at the point $(u, v) \in \Omega$ for all N directions $\theta \in [0, 2\pi]$, we then need to find crossing points of two complex lines of N straight line segments. These crossing points will then be the solutions to (38). The amount of work to do this is proportional to N, by using a monotonic sections algorithm; see e.g. [25]. For all N^2 points on the surface
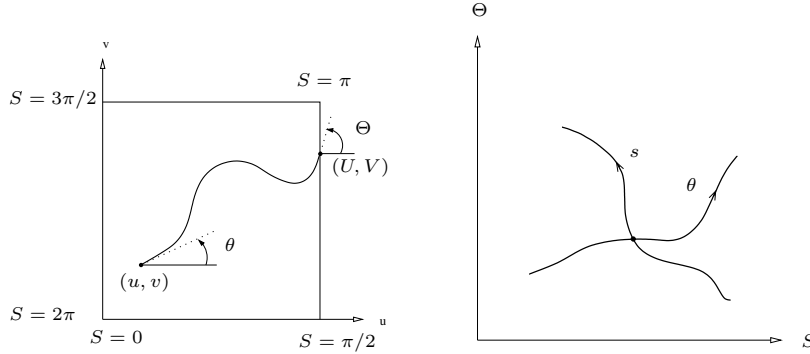
14

Figure 5: Left figure shows a geodesic in a rectangular domain in the parameter space and the choice of S on the boundary. Right figure shows two crossing curves. One curve is for all points on the shadowline, parameterized by s. The other curve is for a single point in the parameter space with all directions, parameterized by θ.

the computational cost for finding crossing points will then be $\mathcal{O}(N^3)$. The complexity to solve the PDEs using the Fast Marching method is $\mathcal{O}(N^3 \log N)$. Therefore the total complexity will be $\mathcal{O}(N^3 \log N)$.

If we only need to compute the field for one shadow line, it could be done faster. For example by using wave front tracking or solvers based on the surface eikonal equation, the complexity is $\mathcal{O}(N^2)$. But there are applications when we need the field for many shadow lines. In such cases, using the Fast Marching method can be much faster. We will show one such application in the next section.

As an example, in Figure 6, the iso-phase curves are shown for an ellipsoid illuminated by incident rays in direction $\hat{I} = [0, 1, 0]$. In the shadow zone between the two shadow lines, there are either one, two or three phases. As it can be seen, multiple phases can be captured. The solution here is computed by the Fast Marching method on a 120^3 grid and using the post-processing described above.

5 An Application to Monostatic RCS Computations

Monostatic RCS is a measure of backscattered radiation in the direction of incident waves, when an object is irradiated. Normally most part of it consists of direct reflections, but for not too high frequencies there are situations where creeping rays can give important contribution [3]. The rays that propagate on the surface of the scatterer and return in the opposite direction of incident waves are called *backscattered creeping rays*.
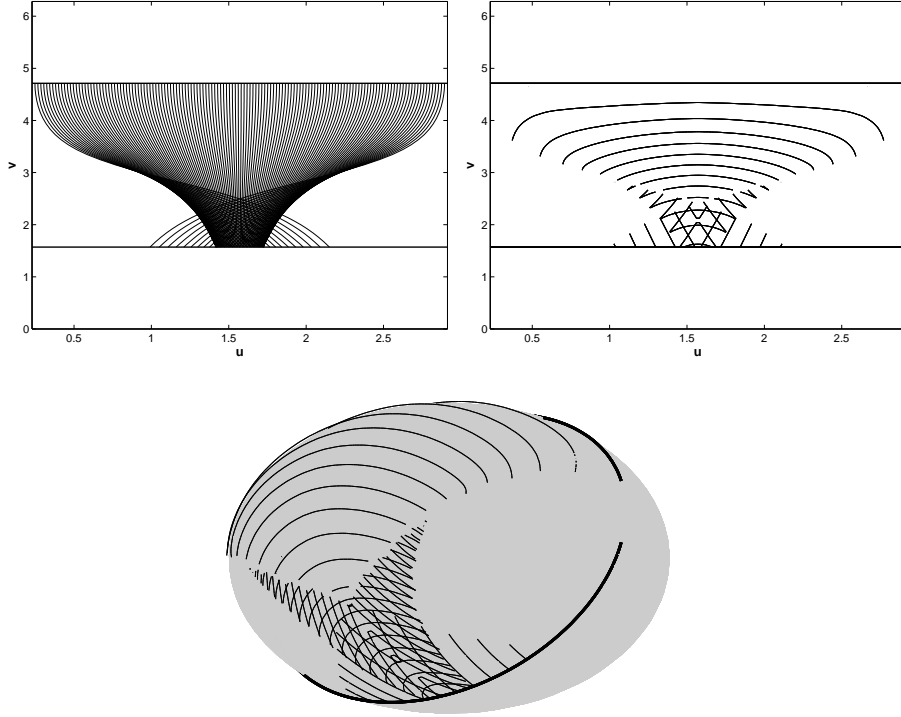
15

Figure 6: Ray propagation on the shadow zone of an ellipsoid. Top figures show the creeping rays (left) and iso-phase curves (right) in the parameter space between two shadow lines. Bottom figure shows the iso-phase curves and the shadow line (bold) in the physical space.

In this section we apply the fast phase space method on a scattering problem and compute the contribution of the backscattered creeping rays to RCS. We compare the results with standard ray tracing.

5.1   Scattering Problem

As a test case we consider a hypersurface $\bar{X} = \bar{X}(u, v)$ which is a patch of an ellipsoid with the following parametric equations:

$$x = -r_1 \cos u,$$
$$y = r_2 \sin u \cos v,$$
$$z = r_3 \sin u \sin v,$$

where $r_1 = 2$, $r_2 = 1$, and $r_3 = 0.5$ are the ellipsoid's semiaxes. Notice that in order to avoid the unregularity at the points $(\pm r_1, 0, 0)$, we cut off these points from the parameter space.

(a) Shadow line in (x, y, z)-space

(b) Shadow line in (u, v)-space
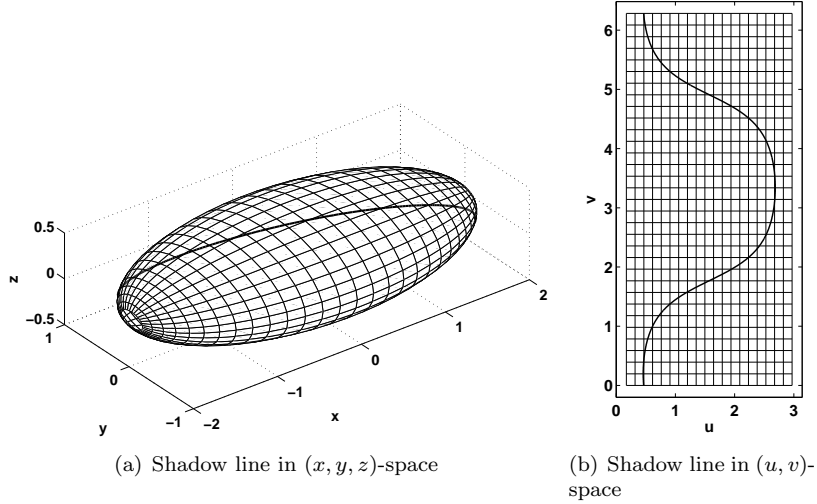
Figure 7: Shadow line in the physical and parameter space.

First, we need to compute the shadow lines on the scatterer. For this hypersurface we can find them analytically. By (7) and (8), the shadow line corresponding to the incident direction $\hat{I} = [\imath_1, \imath_2, \imath_3]$ is given by

$$\imath_1 r_2 r_3 \cos u_0(s) - \imath_2 r_1 r_3 \sin u_0(s) \cos v_0(s) - \imath_3 r_1 r_2 \sin u_0(s) \sin v_0(s) = 0.$$

The ray directions $\theta_0(s)$ at the shadow line are then computed using (39). For example, in Figure 7 the shadow line is shown for $\hat{I} \parallel [0.9, 1, 0.1]$ in physical and parameter space, respectively.

5.2   Finding the Backscattered Rays

The goal is to find the length and amplitude of the backscattered creeping rays for different incident angles. In order to find the backscattered creeping rays, we use postprocessing as before. A backscattered ray starting at point s_1 and ending at point s_2 on shadow line should satisfy

$$F(\gamma(s_1)) = F(\gamma(s_2)) + C, \tag{40}$$

where the constant C acounts for the fact that the upper and lower boundaries in the parameter space coincide on the hypersurface. It means that the points with $S = \pi, \ldots, 3\pi/2$ should be changed to $S = \pi/2, \ldots, 0$ and at the same time their Θ values should be added by π. The reason for adding by π is that we need to reverse the direction of the geodesic starting at s_2. Notice that we only consider the geodesics which hit the upper and lower boundaries, because the left and right boundaries are indeed artificial boundaries, introduced to avoid the unregularity.

17

(a) $F(\gamma(s_1))$ and $F(\gamma(s_2)) + C$ (b) Creeping rays in (u, v) space
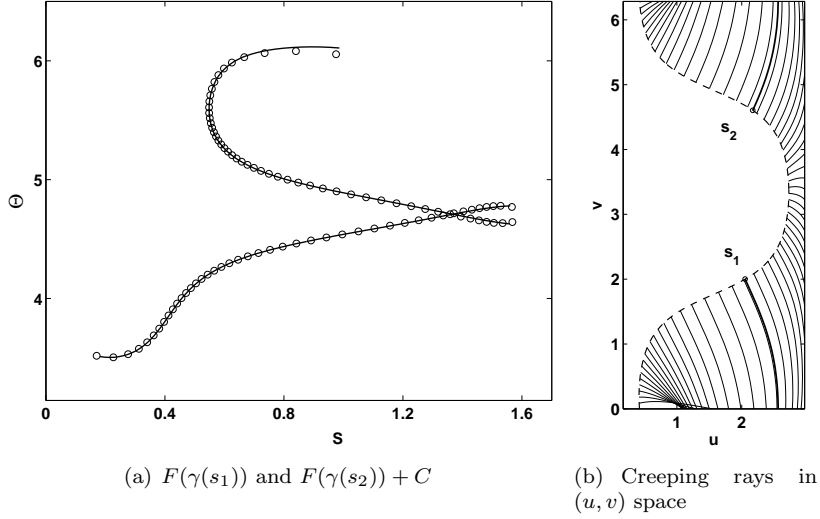
Figure 8: Right figure shows all creeping rays starting at the shadow line (dashed) and ending at the boundary. The two bold curves are the backscattered ray. Left figure shows two curves corresponding to the rays hitting the top and bottom boundaries in the parameter space. Circles denote the values computed by the Fast Marching method and solid lines denote the values computed by a high order accurate ray tracing method. The crossing point corresponds to the backscattered ray.

As before, the right and left hand sides of (40) are curves in $\mathbb{R}^2$ parameterized by s, and to find the backscattered ray we need to find crossing points of these curves. Figure 8(a) shows the intersecting curves in the (S, Θ)-plane for the points on the shadow line corresponding to geodesics hitting the lower and upper boundaries in parameter space, c.f. Figure 5. Figure 8(b) shows the creeping rays starting at all N points on the shadow line and the backscattered ray (bold line).

5.3 Length and Amplitude of Backscattered Ray

The length and amplitude of the backscattered creeping rays are computed by a third order interpolation of the solution to the PDEs (37). Figure 9 shows the length for different incident angles. Figure 10 shows the amplitude for different incident angles and two different frequencies. Note that for computing the amplitude, we only need to compute the geometrical spreading and attenuation of a backscattered creeping ray at the boundary. Therefore we can use the
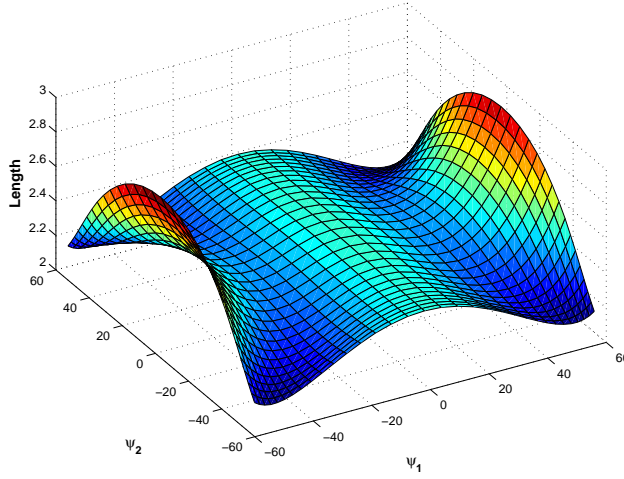
18

Figure 9: Length of the backscattered creeping rays for many illumination angles.

simplified formulation (36). In fact,

$$A(\gamma(s_2)) = A(\gamma(s_1)) \left(\frac{Q(F(\gamma(s_2)))}{Q(F(\gamma(s_1)))} \right)^{\frac{1}{2}} \exp\left(-\omega^{\frac{1}{3}} \left(B(\gamma(s_1)) + B(\gamma(s_2)) \right) \right),$$

For a given incident direction $\hat{I} = [\imath_1, \imath_2, \imath_3]$, the horizontal and vertical incident angles are calculated as

$$\psi_1 = \arctan(\frac{\imath_1}{\imath_2}), \qquad \psi_2 = \arctan(\frac{\imath_3}{\imath_2}).$$

They vary from -60 to 60 degrees. Figure 11 shows the backscattered creeping rays in th physical and parameter space for four different incident directions.

5.4 Convergence and Complexity

We use a first order Fast Marching algorithm. Figure 12 shows the length $\Phi(u, \pi, \pi/2)$ obtained using a coarse mesh of the size 60^3 and a fine mesh of the size 120^3. We compare the solution with a reference solution obtained by a high order accurate Ray tracing method. It confirms the first order accuracy of the Fast Marching algorithm.

The convergence of the length and amplitude (at $\omega = 1$) of the backscattered creeping ray is shown in Figure 13 for a fixed vertical incident angle $\psi_2 = 6$ degree and different horizontal incident angles ψ_1.

The complexity of using the fast phase space method proposed here consists of two parts. First, the cost of solving the PDEs by the Fast Marching method
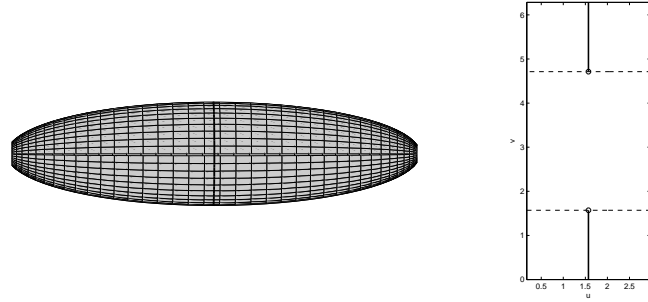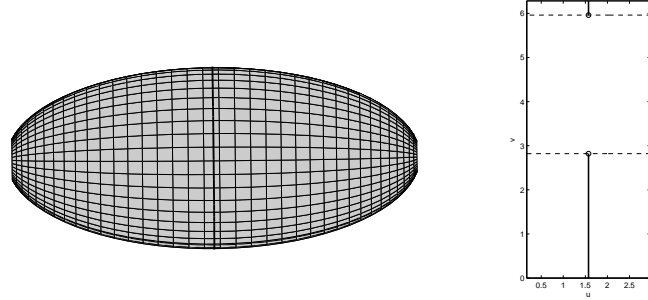
19
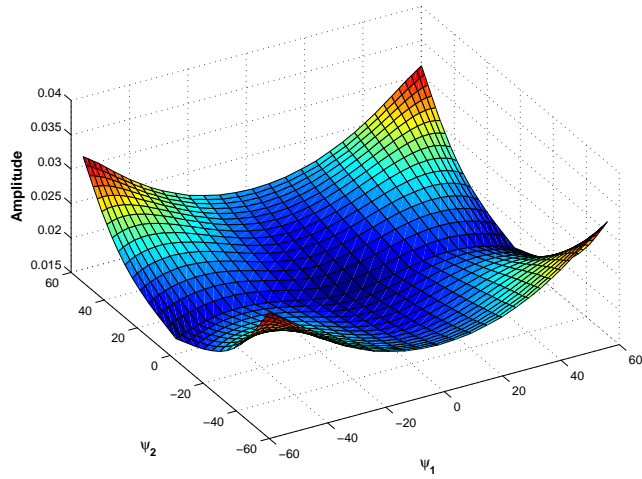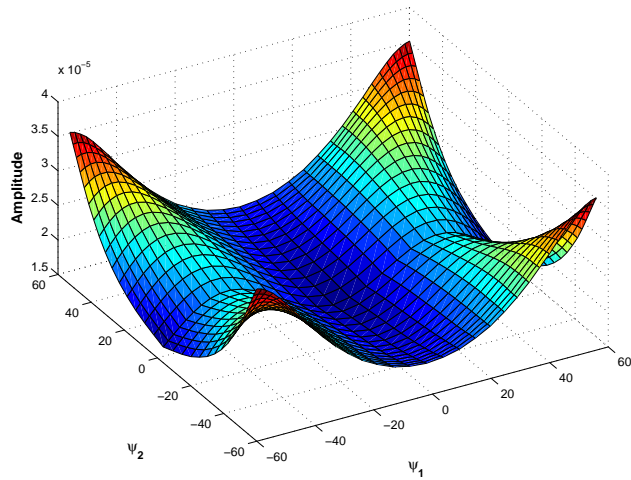
(a) Amplitude, $\omega = 1$
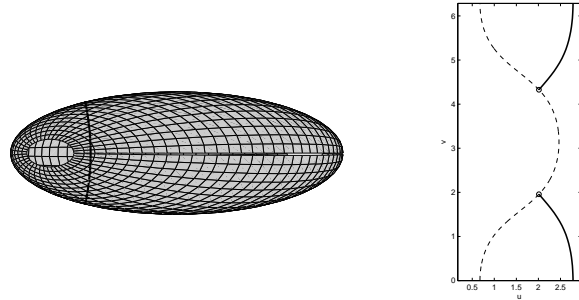

(b) Amplitude, $\omega = 20$

Figure 10: Amplitude of the backscattered creeping rays for many illumination angles and two different frequencies. The frequency determines the balance between the effects of geometrical spreading and attenuation.
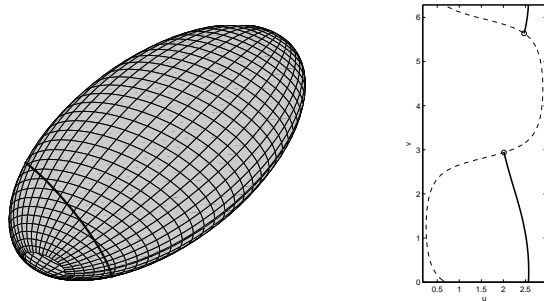
20

(a) $\psi_1 = 0$, $\psi_2 = 0$, length $= 2.44$, $a_1 = 0.017$, $a_{20} = 1.6 \cdot 10^{-5}$

(b) $\psi_1 = 0$, $\psi_2 = 56$, length $= 2.43$, $a_1 = 0.021$, $a_{20} = 1.9 \cdot 10^{-5}$

(c) $\psi_1 = 58$, $\psi_2 = 0$, length $= 2.89$, $a_1 = 0.017$, $a_{20} = 1.6 \cdot 10^{-5}$

(d) $\psi_1 = 58$, $\psi_2 = 56$, length $= 2.16$, $a_1 = 0.032$, $a_{20} = 3.6 \cdot 10^{-5}$

Figure 11: The backscattered creeping rays for four different illumination angles and two different frequencies. Left figures show the backscattered rays in the physical space by bold solid lines. The view direction is in the illumination direction, so that the shadow line is the outer most curve around the ellipsoid. Right figures show the backscattered rays in the parameter space. Shadow lines here are shown by dashed lines. The amplitudes for $\omega = 1$ and $\omega = 20$ are denoted by a_1 and a_{20}, respectively.
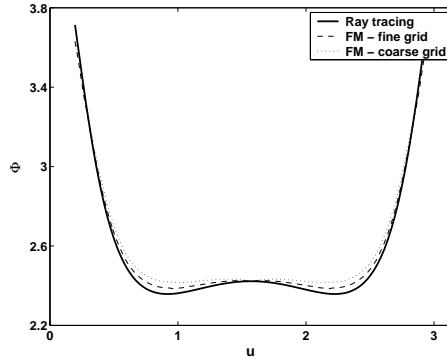
Figure 12: the length $\Phi(u, \pi, \frac{\pi}{2})$ obtained using Fast Marching on a coarse and fine grid. They converge to a reference solution obtanied by a high order solver using Ray tracing.

is $\mathcal{O}(N^3 \log N)$. Second, the cost of finding the backscattered rays for each shadow line is $\mathcal{O}(N)$. For all N^2 shadow lines, it is $\mathcal{O}(N^3)$. Therefore the total complexity will be $\mathcal{O}(N^3 \log N)$. The total cost by using other methods, like wave front tracking and solvers based on the surface eikonal equation, will be $\mathcal{O}(N^4)$, if the cost for each shadow line is $\mathcal{O}(N^2)$. In this case, using the Fast Marching method will then be much faster.

References

[1] J.-D. Benamou. Big ray tracing: Multivalued travel time field computation using viscosity solutions of the eikonal equation. *J. Comput. Phys.*, 128(4):463–474, 1996.

[2] J.-D. Benamou. Direct computation of multivalued phase space solutions for Hamilton-Jacobi equations. *Comm. Pure Appl. Math.*, 52(11):1443–1475, 1999.

[3] D. P. Bouche, J.-J. Bouquet, H. Manenc, and R. Mittra. Asymptotic computation of the RCS of low observable axisymmetric objects at high frequency. *IEEE T. Antenn. Propag.*, 40(10):1165–1174, 1992.

[4] V. Červený, I. A. Molotkov, and I. Psencik. *Ray Methods in Seismology.* Univ. Karlova Press, 1977.

[5] B. Engquist and O. Runborg. Computational high frequency wave propagation. *Acta Numerica*, 12:181–266, 2003.

[6] B. Engquist, O. Runborg, and A.-K. Tornberg. High frequency wave propagation by the segment projection method. *J. Comput. Phys.*, 178:373–390, 2002.
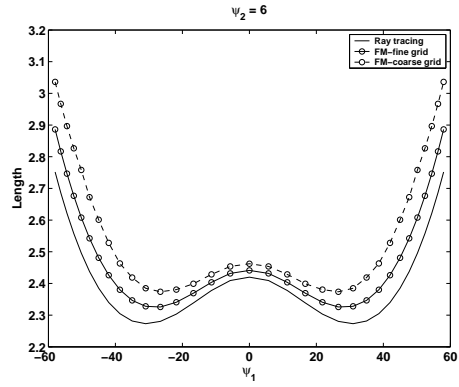
(a) Length
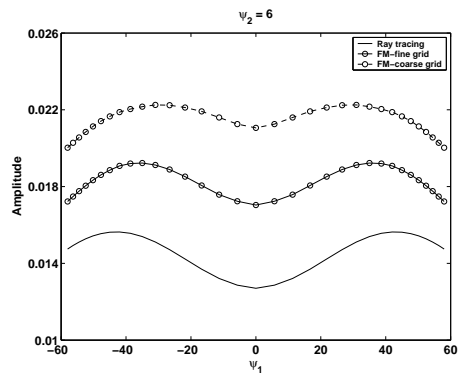
(b) Amplitude

Figure 13: Length and amplitude (at $\omega = 1$) of the backscattered ray for different horizontal incident angles ψ_1 and a fixed vertical incident angle $\psi_2 = 6$. Solutions of Fast Marching algorithm converge to a reference solution obtained by Ray tracing as we use a finer grid.

[7] E. Fatemi, B. Engquist, and S. J. Osher. Numerical solution of the high frequency asymptotic expansion for the scalar wave equation. *J. Comput. Phys.*, 120(1):145–155, 1995.

[8] S. Fomel and J. A. Sethian. Fast phase space computation of multiple arrivals. *Proc. Natl. Acad. Sci. USA*, 99(11):7329–7334 (electronic), 2002.

[9] L. Gosse, S. Jin, and X. Li. Two moment systems for computing multiphase semiclassical limits of the Schrödinger equation. *Math. Models Methods Appl. Sci.*, 13(12):1689–1723, 2003.

[10] A. Gray. *Modern Differential Geometry of Curves and Surfaces*. CRC Press, 1993.

[11] S. Hagdahl. *Hybrid Methods for Computational Electromagnetics in Frequency Domain*. PhD thesis, NADA, KTH, Stockholm, 2005.

[12] P. E. Hussar, V. Oliker, H. L. Riggins, E.M. Smith-Rowlan, W.R. Klocko, and L. Prussner. An implementation of the UTD on facetized CAD platform models. *IEEE Antennas Propag.*, 42(2):100–106, 2000.

[13] J. Keller and R. M. Lewis. Asymptotic methods for partial differential equations: the reduced wave equation and Maxwell's equations. *Surveys Appl. Math.*, 1:1–82, 1995.

[14] R. Kimmel and J. A. Sethian. Computing geodesic paths on manifolds. *Proc. Natl. Acad. Sci. USA*, 95(15):8431–8435 (electronic), 1998.

[15] E. M. Koper, W. D. Wood, and S. W. Schneider. Aircraft antenna coupling minimization using genetic algorithms and approximations. *IEEE T. Aero. Elec. Sys.*, 40(2):742–751, 2004.

[16] Ying L. and E. J. Candes. The phase flow method. Preprint, 2005.

[17] B. R. Levy and J. Keller. Diffraction by a smooth object. *Comm. Pure Appl. Math.*, 12, 1959.

[18] H. Ling, R. Chou, and S. W. Lee. Shooting and bouncing rays: Calculating the RCS of an arbitrarily shaped cavity. *IEEE T. Antenn. Propag.*, 37:194–205, 1989.

[19] R. Mittra. *Topics in Applied Physics: Numerical and Asymptotic Techniques in Electromagnetics*, volume 3. Springer-Verlag, 1975.

[20] S. J. Osher, L.-T. Cheng, M. Kang, H. Shim, and Y.-H. Tsai. Geometric optics in a phase-space-based level set and Eulerian framework. *J. Comput. Phys.*, 179(2):622–648, 2002.

[21] J. Perez, J. A. Saiz, O. M. Conde, R. P. Torre, and M. F. Catedra. Analysis of antennas on board arbitrary structures modeled by NURBS surfaces. *IEEE T. Antenn. Propag.*, 45(6):1045–1053, 1997.

[22] O. Runborg. *Multiphase Computations in Geometrical Optics*. Licentiate's thesis, NADA, KTH, Stockholm, 1996.

[23] O. Runborg. Some new results in multiphase geometrical optics. *M2AN Math. Model. Numer. Anal.*, 34:1203–1231, 2000.

[24] W. W. Symes and J. Qian. A slowness matching Eulerian method for multivalued solutions of eikonal equations. *J. Sci. Comput.*, 19(1-3):501–526, 2003.

[25] G. Taylor. Another look at the line intersection problem. *Int. J. Geogr. Inf. Syst.*, 3(20):192–3, 1989.

[26] J. van Trier and W. W. Symes. Upwind finite-difference calculation of traveltimes. *Geophysics*, 56(6):812–821, June 1991.

[27] J. Vidale. Finite-difference calculation of traveltimes. *B. Seismol. Soc. Am.*, 78(6):2062–2076, December 1988.

[28] V. Vinje, E. Iversen, and H. Gjøystdal. Traveltime and amplitude estimation using wavefront construction. *Geophysics*, 58(8):1157–1166, 1993.